Letter

Breakup of a low-viscosity liquid thread

Hansol Wee, Christopher R. Anthony, and Osman A. Basaran*
Davidson School of Chemical Engineering, Purdue University, West Lafayette, Indiana 47907, USA

(Received 27 July 2022; accepted 3 November 2022; published 23 November 2022)

The thinning of threads of low-viscosity fluids like water in air has been of interest for more than a century and is gaining new importance because of the emergence of applications involving the breakup of drops and jets of liquid metals which have viscosities comparable to but surface tensions and densities much larger than water. The dynamics of thinning and pinch-off is governed by the Ohnesorge number $\mathrm{Oh} = \mu/\sqrt{\rho\gamma R}$, where μ, ρ, γ, and R stand for viscosity, density, surface tension, and nozzle or initial jet radius. When $\mathrm{Oh} \ll 1$, the thread initially thins as if it were inviscid and its minimum radius $\tilde{h}_{\min}$ obeys a universal scaling law $\tilde{h}_{\min} = A(\gamma/\rho)^{1/3}(\tilde{t}_b - \tilde{t})^{2/3}$, where $\tilde{t}_b$ is the time $\tilde{t}$ at which the thread breaks up and $A \doteq 0.717$. As the interface overturns prior to breakup when Oh is sufficiently small, it has proven challenging to observe in simulations and experiments the value of the prefactor A predicted from theory and furthermore the transition of the dynamics as $\tilde{h}_{\min} \to 0$ from the inviscid regime to a different scaling regime in which the effect of viscosity is no longer negligible. Here we employ high-accuracy simulation using a sharp-interface algorithm to show that for sufficiently small Oh, the value of A predicted from computations agrees with the theoretical value to three decimal places and the inviscid power-law behavior can be observed over two to three decades in $\tilde{h}_{\min}$ as $\tilde{t}_b - \tilde{t} \to 0$. Transition out of the inviscid regime and into a viscous one is also demonstrated from simulations.

DOI: 10.1103/PhysRevFluids.7.L112001

I. INTRODUCTION

Thinning and pinch-off of liquid threads or filaments arise during the breakup of liquid jets and drops [1–3] and occur in diverse industrial, natural, and everyday settings including drop-on-demand and continuous inkjet printing [4–6], plasmas produced from molten-tin microdroplets that are used to generate extreme ultraviolet light for nanolithography [7–9], production of particles and capsules [2,10,11], and measurement of physical properties such as surface tension γ [12,13]. While the dynamics of jet and drop breakup for Newtonian fluids has been studied continuously for two centuries [14–19], interest in the physics of thread pinch-off has grown explosively over the past three to four decades since the publication of several landmark papers on the subject [20–23]. Given the growing importance of the breakup of low-viscosity liquid metal jets in state-of-the art applications in semiconductor manufacturing and other industrial settings [8,9,24,25], the goal of this paper is to improve the understanding of the breakup of threads of nearly inviscid fluids.

The thinning of the thread is driven by surface tension or capillary pressure and resisted by inertia and viscous stress. For a thread of an incompressible Newtonian liquid of viscosity μ and density ρ that is surrounded by a dynamically passive gas, e.g., air, breakup occurs in finite time, giving rise to a finite-time singularity [1]. There are three theories that describe pinch-off of Newtonian threads. If fluid viscosity is negligible, breakup is described by an inviscid (or inertial or potential

*obasaran@purdue.edu

flow) scaling theory where surface tension pressure and inertia are in balance as $\tilde{t} \to \tilde{t}_b$, where $\tilde{t}_b$ denotes the time $\tilde{t}$ at which breakup occurs, and the minimum radius of the thread $\tilde{h}_{\min}$ follows the power-law scaling given by [26,27]

$$\tilde{h}_{\min} = A\left(\frac{\gamma}{\rho}\right)^{1/3}(\tilde{t}_b - \tilde{t})^{2/3}. \tag{1}$$

Here A is a universal constant given by $A = 0.717\ldots$ [3,27,28]. If inertia is negligible, breakup is described by a viscous scaling theory in which surface tension and viscous stresses are in balance as the thread tends toward pinch-off and $\tilde{h}_{\min}$ follows the power-law scaling given by [29]

$$\tilde{h}_{\min} = 0.0709\left(\frac{\gamma}{\mu}\right)(\tilde{t}_b - \tilde{t}). \tag{2}$$

When all three forces are important, breakup is described by the inertial-viscous scaling theory of Eggers [22] in which

$$\tilde{h}_{\min} = 0.0304\left(\frac{\gamma}{\mu}\right)(\tilde{t}_b - \tilde{t}). \tag{3}$$

Since neither viscosity nor density can be identically zero or, equivalently, the Ohnesorge number $\mathrm{Oh} \equiv \mu/\sqrt{\rho R\gamma}$, where R is the initial undisturbed radius of a cylindrical column of liquid or tube radius when a drop or a jet is emitted from a nozzle, can be neither zero nor infinite, the inviscid and the viscous scaling regimes are transient ones and only apply during the initial stages of thinning of real threads [30]. Thus, for slightly viscous and highly viscous threads, a transition from these initial regimes takes place to a final or asymptotic inertial-viscous regime as the time remaining until pinch-off $\tilde{\tau} \equiv \tilde{t}_b - \tilde{t} \to 0$ and/or $\tilde{h}_{\min} \to 0$ [30]. In the former case, the transition is expected to occur when $\tilde{h}_{\min}$ becomes comparable to the viscous length $l_\mu \equiv \mu^2/\rho\gamma$ or when $\tilde{h}_{\min}/R \approx \mathrm{Oh}^2$ [2,30,31]. In the latter case, the transition is expected to occur when $\tilde{h}_{\min}/R \approx \mathrm{Oh}^{2/(2\beta-1)}$ [2,30,31], where the exponent $\beta \doteq 0.175$ [29]. Within a few years of the discovery of the three scaling laws and of the possibility of transitions between them, the validity of these laws and possible transitions between them were also demonstrated in a number of computational and experimental studies [32–35]. Thus, by the end of the first decade of the new millennium, the fluid dynamics of Newtonian pinch-off was for all practical purposes considered to be completely worked out [3].

In practice, however, the approach to the pinch-off singularity is more complex, as first anticipated in [31] and demonstrated via detailed simulations and experiments in [36]. Starting in the inviscid (I) regime, low-viscosity threads undergo transitions as $\mathrm{I} \to \mathrm{V} \to \mathrm{IV}$ (V and IV denote viscous and inertial-viscous regimes, respectively) as $\tilde{h}_{\min} \to 0$. Similarly, starting in the viscous regime, high-viscosity threads undergo transitions as $\mathrm{V} \to \mathrm{I} \to \mathrm{V} \to \mathrm{IV}$ as $\tilde{h}_{\min} \to 0$. This complex and slow approach to the asymptotic IV regime during pinch-off was subsequently confirmed by an exceptionally thorough computational study in [37] (see also [38]).

Motivated by applications involving breakup of threads of liquid metals which have viscosities comparable to that of water but surface tensions and densities an order of magnitude larger than those for water [39–43], we address the following questions. First, when $\mathrm{Oh} \ll 1$, we investigate whether the inviscid scaling law not only with the correct scaling exponent but also with the correct value of the universal constant A can be observed in practice. We further probe the occurrence of any possible transitions out of the inviscid regime into a viscous one as $\tilde{h}_{\min} \to 0$ at extremely small values of Oh. The first of these two issues has recently been investigated in a careful computational and experimental study [44]. Here we use a high-accuracy sharp interface algorithm (see, e.g., [45–47]) to probe length and time scales that are several orders of magnitude smaller than those achieved in that pioneering study to provide additional insights and answers to these questions.

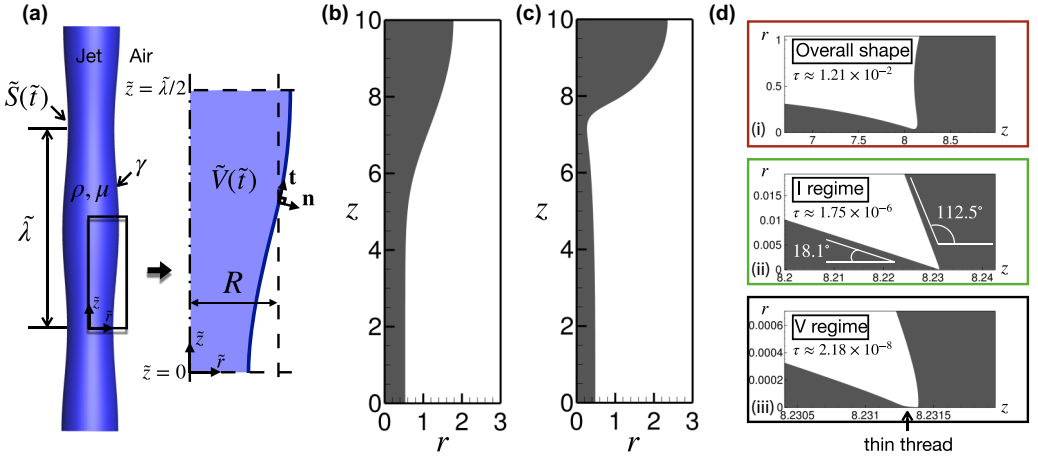

FIG. 1. (a) Definition sketch: an infinitely long liquid column (jet or thread) surrounded by air that is subjected to an axially periodic shape perturbation of wavelength $\tilde{\lambda}$. The inset shows the computational domain, shaded in blue, of axial extent $\tilde{\lambda}/2$. Computed profiles of a thinning liquid jet or thread are shown at (b) $t = 12.035$ and (c) $t = 13.678$. (d) Computed profiles of the jet or thread of (b) and (c) at later times t or smaller τ: (i) overall view of the pinching zone showing the thread and the drop after the interface has already overturned, (ii) zoomed-in view of the interface in the inertial regime, and (iii) zoomed-in view of the interface in the viscous regime. In (b)–(d) Oh $= 0.001$, $\lambda = 20$, and $\epsilon = 0.1$.

II. MATHEMATICAL FORMULATION

The system is isothermal and consists of an infinitely long liquid column (also referred to as a liquid thread or jet) of an incompressible Newtonian fluid of constant density ρ and constant viscosity μ of unperturbed radius R that is surrounded by a dynamically passive ambient gas that simply exerts a constant pressure, which is taken here to be the pressure datum, on the column, as shown in Fig. 1. The surface tension of the liquid-gas (LG) interface is constant and is denoted by γ. The dynamics is taken to be axisymmetric about the centerline of the initially cylindrical column. It thus proves convenient to use a cylindrical coordinate system $(\tilde{r}, \theta, \tilde{z})$ with its origin located along the centerline of the initially cylindrical column and where $\tilde{z}$ is the axial coordinate measured along the column's axis, $\tilde{r}$ is the radial coordinate measured from that axis, and θ is the usual angle measured around the symmetry axis $\tilde{r} = 0$. When subjected to axisymmetric shape perturbations of infinitesimal amplitude whose wavelength in the axial direction is given by $\tilde{\lambda}$, a quiescent cylindrical column of liquid undergoes capillary or Rayleigh-Plateau instability if $\tilde{\lambda} > 2\pi R$ or $\tilde{k}R < 1$, where $\tilde{k} = 2\pi/\tilde{\lambda}$ is the wave number [15,17,48]. In this paper the capillary pinching of a quiescent liquid column is initiated by subjecting its surface $\tilde{S}(\tilde{t})$, where $\tilde{t}$ is time, at time $\tilde{t} = 0$ to a shape perturbation of sufficiently long wavelength but of arbitrary amplitude so that the column's profile is given by

$$\frac{\tilde{r}(\tilde{z}, \tilde{t} = 0)}{R} = \sqrt{1 - \frac{\epsilon^2}{2}} - \epsilon \cos \tilde{k}\tilde{z}. \tag{4}$$

When the disturbance amplitude is small $\epsilon \ll 1$, Eq. (4) simplifies to $\tilde{r}(\tilde{z}, 0)/R = 1 - \epsilon \cos \tilde{k}\tilde{z}$. In what follows, we nondimensionalize the problem by using as characteristic length l_c, time t_c, velocity v_c, and stress T_c the unperturbed jet radius $l_c \equiv R$, inertial-capillary time $t_c \equiv \sqrt{\rho R^3/\gamma}$, inertial-capillary velocity $v_c \equiv \sqrt{\gamma/\rho R}$, and capillary pressure $T_c \equiv \gamma/R$, respectively. Henceforward, variables without tildes are the dimensionless counterparts of variables with tildes, e.g., $\tilde{t}$ and $t \equiv \tilde{t}/t_c$ stand for the dimensional and dimensionless time.

The dynamics of the thinning and breakup of the jet is analyzed by solving the transient free-boundary problem consisting of the continuity and Navier-Stokes equations for fluid velocity $\mathbf{v}$ and pressure p within the jet $V(t)$:

$$\nabla \cdot \mathbf{v} = 0 \quad \text{in } V(t), \tag{5}$$

$$\frac{\partial \mathbf{v}}{\partial t} + (\mathbf{v} \cdot \nabla)\mathbf{v} = \nabla \cdot \mathbf{T} \quad \text{in } V(t). \tag{6}$$

In (6), $\mathbf{T} = -p\mathbf{I} + \mathrm{Oh}[\nabla\mathbf{v} + (\nabla\mathbf{v})^T]$ is the total stress tensor for a Newtonian fluid, $\mathbf{I}$ is the identity tensor, and $\mathrm{Oh} \equiv \mu/\sqrt{\rho R\gamma}$ is the Ohnesorge number.

As (5) and (6) are balances of mass and momentum conservation in the bulk $V(t)$, the corresponding principles of mass and momentum conservation at the LG interface $S(t)$ are the kinematic and traction boundary conditions [49–52]. In the absence of bulk flow or mass transfer across the interface [51], the kinematic boundary condition is given by [51,52]

$$\mathbf{n} \cdot (\mathbf{v} - \mathbf{v}_s) = 0 \quad \text{on } S(t), \tag{7}$$

where $\mathbf{v}_s$ is the velocity of points on the interface and $\mathbf{n}$ is the outward pointing unit normal to $S(t)$. The traction or the stress-balance boundary condition at the free surface is given by [51,52]

$$\mathbf{n} \cdot \mathbf{T} = 2\mathcal{H}\mathbf{n} \quad \text{on } S(t), \tag{8}$$

where $2\mathcal{H} \equiv -\nabla \cdot \mathbf{n}$ is twice the mean curvature of the free surface.

Because the dynamics is axisymmetric about the z axis, the shear stress and the radial velocity have to vanish along the centerline ($r = 0$), viz., $\mathbf{e}_r \cdot \mathbf{T} \cdot \mathbf{e}_z = 0$ and $u \equiv \mathbf{v} \cdot \mathbf{e}_r = 0$, where $\mathbf{e}_r$ and $\mathbf{e}_z$ stand for the unit vectors in the radial and axial directions, respectively. On account of the periodicity of the imposed initial perturbation of the jet's surface, the problem only needs to be solved over an axial distance equal to one-half of the wavelength of the imposed perturbation. Thus, along the two symmetry planes located at $z = 0$ and $z = \pi/k = \lambda/2$, both the shear stress and the axial velocity must vanish, viz., $\mathbf{e}_z \cdot \mathbf{T} \cdot \mathbf{e}_r = 0$ and $v \equiv \mathbf{v} \cdot \mathbf{e}_z = 0$. Also because of periodicity, the interface profile must obey $\mathbf{e}_r \cdot \mathbf{t} = 0$, where $\mathbf{t}$ is the unit tangent to $S(t)$, at $z = 0$ and $z = \pi/k$.

III. NUMERICAL ANALYSIS

The transient system of three-dimensional but axisymmetric (3DA) equations (5) and (6) is solved numerically by means of a fully implicit, arbitrary Lagrangian-Eulerian method-of-lines algorithm in which the Galerkin finite-element method is used for spatial discretization [53–56] and an adaptive, implicit finite-difference method is employed for time integration [54,57–61]. As jet breakup is a free-boundary problem that involves a highly deformable LG interface, an elliptic mesh generation technique [62] is employed to track the moving boundary and determine the radial and axial coordinates of each grid point in the moving, adaptive mesh simultaneously with the velocity and pressure unknowns in the jet as well as the free-surface profile. In the 3DA sharp-interface algorithm, the free surface is parametrized in terms of arc length s (see, e.g., [34,60,63]). This parametrization, as opposed to using one where the interface shape is a single-valued function of the axial coordinate, coupled to the elliptic mesh generation algorithm allows simulation of jet dynamics in which the interface may overturn [34,60,63]. At each time step, the resulting system of nonlinear algebraic equations is solved iteratively using Newton's method where the Jacobian is computed analytically. The large system of linear equations at each iteration is solved by means of a direct solver using Gaussian elimination and a multifrontal algorithm [64] based on the frontal solver concept developed by Hood [65]. We have used similar versions of the algorithm over the past two decades to analyze the breakup of jets, drops, and filaments [34,45,47,63,66–68].

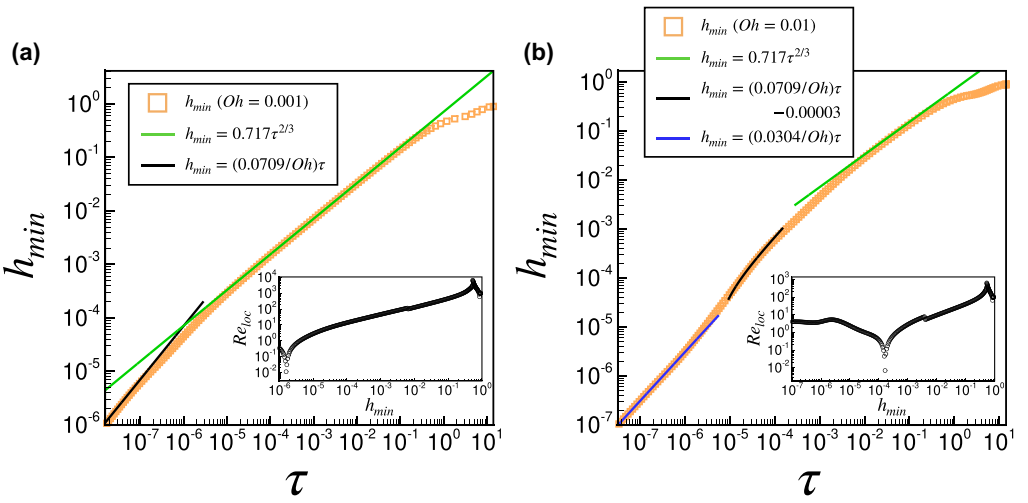

FIG. 2. Variation of the minimum thread radius $h_{\min}$ with time remaining until pinch-off τ: (a) Oh = 0.001 and (b) Oh = 0.01. Orange squares represent the simulation data, green lines show the inertial scaling law, black lines show the viscous scaling law, and the blue line shows the inertial-viscous scaling law. The insets show the variation of the local Reynolds number $\mathrm{Re}_{\mathrm{loc}}$ with $h_{\min}$. Here $\lambda = 20$ and $\epsilon = 0.1$.

IV. RESULTS

In this section we report the results of simulations carried out when initially quiescent liquid columns are subjected to perturbations of amplitude $\epsilon = 0.1$ and dimensionless wavelength $\lambda = 20$. It should be noted that when a water jet issues out of a capillary tube of 1 mm radius, $\mathrm{Oh} = 3.7 \times 10^{-3}$. If the tube radius were decreased by two orders of magnitude to 10 μm, we would obtain a value that is typical of modern inkjet printers [2,4–6], $\mathrm{Oh} = 3.7 \times 10^{-2}$. In [44] the authors report results in a number of situations including the breakup of mercury bridges of $\mathrm{Oh} = 6.0437 \times 10^{-4}$. Therefore, we have picked $\mathrm{Oh} = 2 \times 10^{-3}$, 10^{-3}, 5×10^{-4}, and 2.5×10^{-4}, in which the value of Oh is systematically halved to probe the dynamics of breakup for nearly inviscid fluids. We have also considered two additional situations, one with $\mathrm{Oh} = 2.6 \times 10^{-3}$ to provide a direct comparison with [44] and another with $\mathrm{Oh} = 10^{-2}$ where the Ohnesorge number is comparable to the inkjet example given above. In much of the discussion to follow, we present results on how the minimum jet radius $h_{\min} \equiv \tilde{h}_{\min}/R$ or the prefactor A varies with time remaining until rupture $\tau \equiv \tilde{\tau}/t_c = (\tilde{t}_b - \tilde{t})/t_c = t_b - t$.

Figures 1(b)–(d) show the profiles of a jet of $\mathrm{Oh} = 10^{-3}$ at five instances in time. Following the imposition of the initial perturbation, the column deforms at early times such that its radius is a minimum at $z = 0$ [Fig. 1(b)]. However, the location of the minimum radius $h_{\min}$ migrates from $z = 0$ due to inertia as shown in Figs. 1(c) and 1(d i), in accord with previous studies [36]. As the jet continues to thin, the interface overturns in the vicinity of $h_{\min}$ and the interface profile resembles two cones that meet in the neighborhood of that location [27,69,70]. A zoomed-in view of the jet profile in the vicinity of $h_{\min}$ is shown in Fig. 1(d ii). Here the computed cone angles of 18.1° for the shallow cone and 112.5° for the overturned steep cone are in excellent agreement with results of boundary integral simulations [27,69] and experiments [70]. As $h_{\min}$ continues to decrease, a thin thread forms which connects the thread side of the jet to its drop side [Fig. 1(d iii)].

Figure 2 shows the computed variation of the minimum neck radius $h_{\min}$ with time remaining until pinch-off τ when $\mathrm{Oh} = 0.001$ [Fig. 2(a)] and $\mathrm{Oh} = 0.01$ [Fig. 2(b)] and the variation of the local Reynolds number $\mathrm{Re}_{\mathrm{loc}} = v'z'/\mathrm{Oh}$ (here v' and z' stand for the characteristic axial velocity in and axial extent of the pinching zone, respectively) [36] with $h_{\min}$ as insets in both cases. Figure 2(a) makes plain that after the decay of initial transients, the computed variation of $h_{\min}$ with τ follows

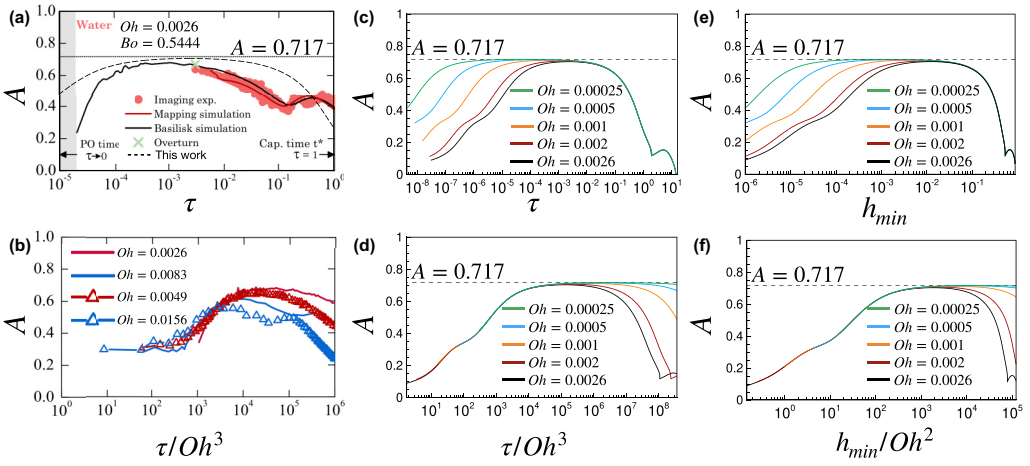

FIG. 3. Variation of the prefactor A with time remaining until pinch-off τ, rescaled time until pinch-off τ/Oh^3, minimum thread radius $h_{\min}$, and rescaled minimum radius $h_{\min}/\mathrm{Oh}^2$ (see the text). (a) and (b) Results from dripping studies of [44], except for the dashed curve labeled "This work" in (a). (c)–(f) Results obtained with the sharp-interface algorithm of this paper when $\lambda = 20$ and $\epsilon = 0.1$. Our simulation results for $\mathrm{Oh} = 0.0026$ are also shown in (a) for a side-by-side comparison with [44]. The difference between the two sets of results at early times (or large τ) can be attributed to the different physical problems studied in [44] and here.

the inviscid scaling law (1) over several decades of variation in these variables. Figure 2(a) further shows that when $h_{\min} \approx 10^{-5}$, the dynamics begins to transition into the viscous regime where the variation of $h_{\min}$ with τ is dictated by (2). In Fig. 2(b), on account of the fact that Oh is an order of magnitude larger than that in Fig. 2(a), the duration of the I regime is too short but the dynamics even exhibits a transition to an intermediate V regime that is then followed by a final transition to the asymptotic IV regime as $h_{\min} \to 0$. We note that in both Figs. 2(a) and 2(b) it is shown from the insets that the inertial regime is exited when $\mathrm{Re}_{\mathrm{local}}$ becomes sufficiently small.

Figure 3 shows the variation of the prefactor A with time remaining until pinch-off reported in [44] [Figs. 3(a) and 3(b)] and the evolution of A obtained with our sharp-interface algorithm [Figs. 3(c)–3(f)]. Following [37] and as in [44], we determine A from the slope of $h_{\min}^{3/2} = A^{3/2}\tau = A^{3/2}(t_b - t)$ versus time [cf. Eq. (1)] which does not require knowledge of and/or sidesteps the estimation of the breakup time by extrapolation. The results of Figs. 3(c) and 3(e) make plain that as $\mathrm{Oh} \to 0$, not only does the computed value of A approach the theoretical value of $A \doteq 0.717$ but the system follows the inviscid scaling law over several decades of variation in τ and/or $h_{\min}$. The new simulations predict that when $\mathrm{Oh} = 5 \times 10^{-4}$, $A = 0.713$, which is within 0.6% of the value predicted from theory, and that when $\mathrm{Oh} = 2.5 \times 10^{-4}$, $A = 0.717$, which agrees with the theoretical value to three decimal places. A comparison of the new results of Fig. 3(c) with those of Fig. 3(a) makes plain that the sharp-interface algorithm of this paper has achieved a number of improvements with respect to the earlier results: The curve depicting the variation of A with τ determined by the present sharp-interface algorithm is devoid of wiggles, the time period over which the inviscid regime is observed is much longer, and a more accurate prediction has been made of the value of A.

As $h_{\min}$ continues to decrease, viscous effects come into the picture, as shown in Fig. 2. In Ref. [44] the authors illustrate this fact by replotting the time evolution of the prefactor as A versus time remaining until pinch-off nondimensionalized by the viscous time $t_\mu \equiv \mu^3/\rho\gamma^2$, viz., $\tilde{\tau}/t_\mu \equiv \tau/\mathrm{Oh}^3$. Figure 3(b) and 3(d) show the variation of A with τ/Oh^3 reported in [44] and determined with the algorithm of this paper. Additionally, we show in Fig. 3(f) the variation of A with the minimum thread radius nondimensionalized by the viscous length $l_\mu = \mu^2/\rho\gamma$, viz.,

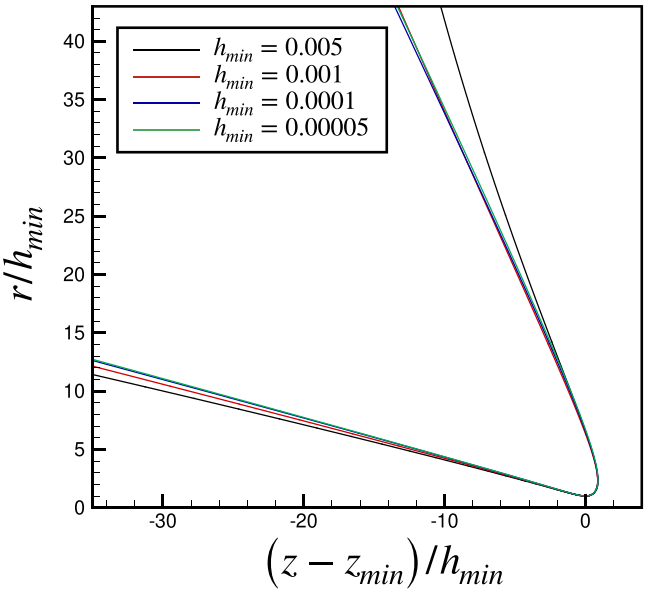

FIG. 4. Suitably rescaled interface shapes in the vicinity of the minimum thread radius, which is located at $(r, z) = (h_{\min}, z_{\min})$, obtained from simulations that show the collapse of the shapes onto the double-cone inviscid similarity profile. The two curves corresponding to the two smallest values of $h_{\min}$ are nearly indistinguishable as they virtually fall on top of one another. Here $\mathrm{Oh} = 5 \times 10^{-4}$, $\lambda = 20$, and $\epsilon = 0.1$.

$\tilde{h}_{\min}/l_\mu \equiv h_{\min}/\mathrm{Oh}^2$. Whereas the data far from pinch-off collapse onto one curve when A is plotted against τ or $h_{\min}$, the data near pinch-off collapse nicely onto one master curve when A is plotted against τ/Oh^3 or $h_{\min}/\mathrm{Oh}^2$.

When the system is in the inviscid regime and before it transitions out of that regime into the viscous regime, the interface profiles in the vicinity of $h_{\min}$ can be suitably collapsed to illustrate not only the self-similarity of the dynamics but also the double-cone structure that is now well known from theory, simulations, and experiments. Figure 4 shows these collapsed shapes obtained with the new algorithm when $\mathrm{Oh} = 5 \times 10^{-4}$. We also note that these shapes too are devoid of wiggles even at the latest times in contrast to the earlier work by Deblais *et al.* [44].

V. CONCLUSION

The topic of the thinning and pinch-off of liquid threads of Newtonian fluids has remained a rich and rewarding subject despite nearly 200 years of continuous study (see, e.g., [1,2,14,15,17,71]). The results presented in this paper on certain details of the flow in the vicinity of the pinch-off singularity for low-viscosity or nearly inviscid fluids are especially relevant and timely given the growing interest in the breakup of drops and jets of liquid metals [7–9,24,43].

According to the foregoing results and especially those presented in Figs. 2 and 3, liquid drops and jets of $\mathrm{Oh} \leqslant 10^{-3}$ thin as if the fluid were inviscid as the minimum radius of the drop or jet falls by four (or more) orders of magnitude from macroscopic to molecular scales. In the experiments with mercury carried out in [35], $l_\mu = 0.35$ nm. Therefore, if the initial jet radius in Fig. 2 were $R = 350$ μm, viscous effects would be negligible until the minimum neck radius of a thinning mercury jet fell by about five orders of magnitude or below 3.5 nm, which is of the order of the limit of applicability of continuum mechanics. Burton *et al.* [35] found that the mercury bridges in their experiments followed the inviscid scaling law with the 2/3 power-law exponent until the minimum neck radius fell to about a few nanometers. In conclusion, it would be both physically realistic and

computationally efficient to model the dynamics of drop and jet breakup when Oh $\ll 1$ by treating the fluid as inviscid and using a potential flow code [27,58,59,69].

ACKNOWLEDGMENTS

We gratefully acknowledge financial support from the Gedge Professorship to O.A.B. and the Purdue Process Safety and Assurance Center.

[1] J. Eggers, Nonlinear dynamics and breakup of free-surface flows, Rev. Mod. Phys. **69**, 865 (1997).
[2] O. A. Basaran, Small-scale free surface flows with breakup: Drop formation and emerging applications, AIChE J. **48**, 1842 (2002).
[3] J. Eggers and E. Villermaux, Physics of liquid jets, Rep. Prog. Phys. **71**, 036601 (2008).
[4] O. A. Basaran, H. Gao, and P. P. Bhat, Nonstandard inkjets, Annu. Rev. Fluid Mech. **45**, 85 (2013).
[5] A. A. Castrejón-Pita, E. S. Betton, N. Campbell, N. Jackson, J. Morgan, T. R. Tuladhar, D. C. Vadillo, and J. R. Castrejon-Pita, Formulation, quality, cleaning, and other advances in inkjet printing, Atomization Spray. **31**, 57 (2021).
[6] D. Lohse, Fundamental fluid dynamics challenges in inkjet printing, Annu. Rev. Fluid Mech. **54**, 349 (2022).
[7] V. Y. Banine, K. N. Koshelev, and G. H. P. M. Swinkels, Physical processes in EUV sources for microlithography, J. Phys. D **44**, 253001 (2011).
[8] O. O. Versolato, Physics of laser-driven tin plasma sources of EUV radiation for nanolithography, Plasma Sources Sci. Technol. **28**, 083001 (2019).
[9] O. Versolato, J. Sheil, S. Witte, W. Ubachs, and R. Hoekstra, Microdroplet-tin plasma sources of EUV radiation driven by solid-state-lasers (topical review), J. Opt. **24**, 054014 (2022).
[10] Y. Yeo, A. U. Chen, O. A. Basaran, and K. Park, Solvent exchange method: A novel microencapsulation technique using dual microdispensers, Pharm. Res. **21**, 1419 (2004).
[11] D. Lohse and X. Zhang, Physicochemical hydrodynamics of droplets out of equilibrium, Nat. Rev. Phys. **2**, 426 (2020).
[12] X. Zhang, M. T. Harris, and O. A. Basaran, Measurement of dynamic surface tension by a growing drop technique, J. Colloid Interf. Sci. **168**, 47 (1994).
[13] S. M. I. Saad, Z. Policova, and A. W. Neumann, Design and accuracy of pendant drop methods for surface tension measurement, Colloid. Surf. A **384**, 442 (2011).
[14] F. Savart, Mémoires sur la constitution des veines liquides lancées par des orifices circulaires en mince paroi, Ann. Chim. Phys. **53**, 337 (1833).
[15] J. A. F. Plateau, *Experimental and Theoretical Statics of Liquids Subject to Molecular Forces Only* (Gauthier-Villars, Paris, 1873).
[16] P. Lenard, Ueber die schwingungen fallender tropfen, Ann. Phys. **266**, 209 (1887).
[17] L. Rayleigh, On the instability of jets, Proc. London Math. Soc. **s1-10**, 4 (1878).
[18] L. Rayleigh, XIX. On the instability of cylindrical fluid surfaces, Philos. Mag. **34**, 177 (1892).
[19] H. E. Edgerton, E. A. Hauser, and W. B. Tucker, Studies in drop formation as revealed by the high-speed motion camera, J. Phys. Chem. **41**, 1017 (1937).
[20] J. B. Keller and M. J. Miksis, Surface tension driven flows, SIAM J. Appl. Math. **43**, 268 (1983).
[21] D. H. Peregrine, G. Shoker, and A. Symon, The bifurcation of liquid bridges, J. Fluid Mech. **212**, 25 (1990).
[22] J. Eggers, Universal Pinching of 3D Axisymmetric Free-Surface Flow, Phys. Rev. Lett. **71**, 3458 (1993).
[23] X. D. Shi, M. P. Brenner, and S. R. Nagel, A cascade of structure in a drop falling from a faucet, Science **265**, 219 (1994).
[24] J. De Groot, G. A. Johansson, and H. M. Hertz, Capillary nozzles for liquid-jet laser-plasma x-ray sources, Rev. Sci. Instrum. **74**, 3881 (2003).

[25] C. Ladd, J.-H. So, J. Muth, and M. D. Dickey, 3D printing of free standing liquid metal microstructures, Adv. Mater. **25**, 5081 (2013).
[26] Y. J. Chen and P. H. Steen, Dynamics of inviscid capillary breakup: Collapse and pinchoff of a film bridge, J. Fluid Mech. **341**, 245 (1997).
[27] R. F. Day, E. J. Hinch, and J. R. Lister, Self-Similar Capillary Pinchoff of an Inviscid Fluid, Phys. Rev. Lett. **80**, 704 (1998).
[28] D. Leppinen and J. R. Lister, Capillary pinch-off in inviscid fluids, Phys. Fluids **15**, 568 (2003).
[29] D. T. Papageorgiou, On the breakup of viscous liquid threads, Phys. Fluids **7**, 1529 (1995).
[30] J. R. Lister and H. A. Stone, Capillary breakup of a viscous thread surrounded by another viscous fluid, Phys. Fluids **10**, 2758 (1998).
[31] J. Eggers, Drop formation—An overview, ZAMM—J. Appl. Math. Mech. **85**, 400 (2005).
[32] P. K. Notz, A. U. Chen, and O. A. Basaran, Satellite drops: Unexpected dynamics and change of scaling during pinch-off, Phys. Fluids **13**, 549 (2001).
[33] A. Rothert, R. Richter, and I. Rehberg, Transition from Symmetric to Asymmetric Scaling Function before Drop Pinch-Off, Phys. Rev. Lett. **87**, 084501 (2001).
[34] A. U. Chen, P. K. Notz, and O. A. Basaran, Computational and Experimental Analysis of Pinch-Off and Scaling, Phys. Rev. Lett. **88**, 174501 (2002).
[35] J. C. Burton, J. E. Rutledge, and P. Taborek, Fluid Pinch-Off Dynamics at Nanometer Length Scales, Phys. Rev. Lett. **92**, 244505 (2004).
[36] J. R. Castrejón-Pita, A. A. Castrejón-Pita, S. S. Thete, K. Sambath, I. M. Hutchings, J. Hinch, J. R. Lister, and O. A. Basaran, Plethora of transitions during breakup of liquid filaments, Proc. Natl. Acad. Sci. USA **112**, 4582 (2015).
[37] Y. Li and J. E. Sprittles, Capillary breakup of a liquid bridge: Identifying regimes and transitions, J. Fluid Mech. **797**, 29 (2016).
[38] A. Lagarde, C. Josserand, and S. Protière, Oscillating path between self-similarities in liquid pinch-off, Proc. Natl. Acad. Sci. USA **115**, 12371 (2018).
[39] L. L. Bircumshaw, XXVIII. The surface tension of liquid metals. Part I. Tin and lead, Philos. Mag. **2**, 341 (1926).
[40] L. L. Bircumshaw, XIV. The surface tension of liquid metals. Part V. The surface tension of the lead-tin alloys, Philos. Mag. **17**, 181 (1934).
[41] B. J. Keene, Review of data for the surface tension of pure metals, Int. Mater. Rev. **38**, 157 (1993).
[42] M. Song, K. E. Daniels, A. Kiani, S. Rashid-Nadimi, and M. D. Dickey, Interfacial tension modulation of liquid metal via electrochemical oxidation, Adv. Intell. Syst. **3**, 2100024 (2021).
[43] M. D. Dickey, Liquid metals at room temperature, Phys. Today **74**(4), 30 (2021).
[44] A. Deblais, M. A. Herrada, I. Hauner, K. P. Velikov, T. van Roon, H. Kellay, J. Eggers, and D. Bonn, Viscous Effects on Inertial Drop Formation, Phys. Rev. Lett. **121**, 254501 (2018).
[45] C. R. Anthony, P. M. Kamat, M. T. Harris, and O. A. Basaran, Dynamics of contracting filaments, Phys. Rev. Fluids **4**, 093601 (2019).
[46] P. M. Kamat, B. W. Wagoner, A. A. Castrejón-Pita, J. R. Castrejón-Pita, C. R. Anthony, and O. A. Basaran, Surfactant-driven escape from endpinching during contraction of nearly inviscid filaments, J. Fluid Mech. **899**, A28 (2020).
[47] C. R. Anthony, H. Wee, V. Garg, S. S. Thete, P. M. Kamat, B. W. Wagoner, E. D. Wilkes, P. K. Notz, A. U. Chen, R. Suryo, K. Sambath, J. C. Panditaratne, Y.-C. Liao, and O. A. Basaran, Sharp interface methods for simulation and analysis of free surface flows with singularities: Breakup and coalescence, Annu. Rev. Fluid Mech. **55**, 707 (2023).
[48] D. H. Michael, Meniscus stability, Annu. Rev. Fluid Mech. **13**, 189 (1981).
[49] R. Aris, *Vectors, Tensors and the Basic Equations of Fluid Mechanics* (Courier, Chelmsford, 2012).
[50] L. E. Scriven, Dynamics of a fluid interface equation of motion for newtonian surface fluids, Chem. Eng. Sci. **12**, 98 (1960).
[51] W. M. Deen, *Analysis of Transport Phenomena* (Oxford University Press, New York, 1998), Vol. 2.
[52] L. G. Leal, *Advanced Transport Phenomena: Fluid Mechanics and Convective Transport Processes* (Cambridge University Press, Cambridge, 2007), Vol. 7.

[53] P. M. Gresho and R. L. Sani, *Incompressible Flow and the Finite Element Method* (Wiley, New York, 1998), Vol. 1.
[54] M. S. Gockenbach, *Understanding and Implementing the Finite Element Method* (SIAM, Philadelphia, 2006).
[55] O. A. Basaran, Nonlinear oscillations of viscous liquid drops, J. Fluid Mech. **241**, 169 (1992).
[56] J. Q. Feng and O. A. Basaran, Shear flow over a translationally symmetric cylindrical bubble pinned on a slot in a plane wall, J. Fluid Mech. **275**, 351 (1994).
[57] P. M. Gresho, R. L. Lee, and R. C. Sani, in *Recent Advances Numerical Methods in Fluids*, edited by C. Taylor and K. Morgan (Pineridge, Swansea, 1980), pp. 27–79.
[58] T. W. Patzek, R. E. Benner, Jr., O. A. Basaran, and L. E. Scriven, Nonlinear oscillations of inviscid free drops, J. Comput. Phys. **97**, 489 (1991).
[59] O. A. Basaran, T. W. Patzek, R. E. Benner, Jr., and L. E. Scriven, Nonlinear oscillations and breakup of conducting, inviscid drops in an externally applied electric field, Ind. Eng. Chem. Res. **34**, 3454 (1995).
[60] E. D. Wilkes, S. D. Phillips, and O. A. Basaran, Computational and experimental analysis of dynamics of drop formation, Phys. Fluids **11**, 3577 (1999).
[61] E. D. Wilkes and O. A. Basaran, Drop ejection from an oscillating rod, J. Colloid Interf. Sci. **242**, 180 (2001).
[62] K. N. Christodoulou and L. E. Scriven, Discretization of free surface flows and other moving boundary problems, J. Comput. Phys. **99**, 39 (1992).
[63] P. K. Notz and O. A. Basaran, Dynamics and breakup of a contracting liquid filament, J. Fluid Mech. **512**, 223 (2004).
[64] C. R. Anthony, Dynamics of retracting films and filaments near singularities, Ph.D. thesis, Purdue University, 2017.
[65] P. Hood, Frontal solution program for unsymmetric matrices, Int. J. Numer. Methods Eng. **10**, 379 (1976).
[66] C. R. Anthony, M. T. Harris, and O. A. Basaran, Initial regime of drop coalescence, Phys. Rev. Fluids **5**, 033608 (2020).
[67] H. Wee, B. W. Wagoner, V. Garg, P. M. Kamat, and O. A. Basaran, Pinch-off of a surfactant-covered jet, J. Fluid Mech. **908**, A38 (2021).
[68] B. W. Wagoner, P. M. Vlahovska, M. T. Harris, and O. A. Basaran, Electrohydrodynamics of lenticular drops and equatorial streaming, J. Fluid Mech. **925**, A36 (2021).
[69] J. C. Burton and P. Taborek, Two-dimensional inviscid pinch-off: An example of self-similarity of the second kind, Phys. Fluids **19**, 102109 (2007).
[70] J. R. Castrejón-Pita, A. A. Castrejón-Pita, E. J. Hinch, J. R. Lister, and I. M. Hutchings, Self-similar breakup of near-inviscid liquids, Phys. Rev. E **86**, 015301(R) (2012).
[71] F. Cruz-Mazo and H. A. Stone, Pinch-off of liquid jets at the finite scale of an interface, Phys. Rev. Fluids **7**, L012201 (2022).